Elastic constants of $KMnF_3$ as functions of temperature and pressure

Wenwu Cao and Gerhard R. Barsch
Materials Research Laboratory and Department of Physics, The Pennsylvania State University, University Park, Pennsylvania 16802
(Received 21 March 1988)

We have measured the single-crystal elastic constants of $KMnF_3$ and their first pressure derivatives from 200 to 430 K at a frequency of 20 MHz by means of the ultrasonic-pulse-superposition method. Both sets of data show cusplike anomalies above the improper O_h-D_{4h} ferroelastic transition at 186 K that extend up to 350 K. Above 350 K the temperature dependence is linear, making it possible to determine the bare harmonic and anharmonic constants by means of linear extrapolation to $T=0$. At room temperature the second pressure derivatives of the elastic constants were also measured. Analysis of the data on the basis of a model with Coulomb and short-range central force interactions indicates anomalously large fourth derivatives of the Mn-F and F-F pair potentials. A calculation of the temperature dependence of the elastic Grüneisen parameter is consistent with models for the acoustic anomaly according to which coupling between strains and order-parameter fluctuations is limited to frequencies less than the relaxation rate of the soft R_{25} mode.

I. INTRODUCTION

Starting with the discovery of ferroelectricity in $BaTiO_3$ in 1945,[1] and stimulated by the introduction of the soft-mode concept,[2,3] ternary compounds of composition ABX_3 occurring in the perovskite structure have probably become the most thoroughly studied class of materials.[4,5] Interest originated both in their great importance for electromechanical and electrooptic device applications[4] and in the rich variety of physical phenomena associated with displacive phase transitions driven by soft phonon modes occurring at different high-symmetry points of the Brillouin zone.[4,6,7] Following the discovery of high-T_c superconductivity in perovskite-based layer-type oxides[8,9] interest in this class of materials has surged recently.

The present work was motivated by the fact that even the most detailed microscopic theory of mode softening in perovskites available to date, that of Bruce and Cowley,[10] utilizes empirical input parameters that are very uncertain. These authors extended the harmonic rigid shell model of Stirling[11] by including short-range anharmonic interactions and showed by means of many-body perturbation theory that the two soft modes Γ_{15} and R_{25} observed in $SrTiO_3$ arise from anharmonic phonon-phonon interactions.[10] The temperature dependence of the R_{25} mode frequency is determined by the sum of $\Delta^{(3)}$ and $\Delta^{(4)}$, representing the contributions to the real part of the anharmonic self-energy from the third- and fourth-order coupling parameters, respectively, which are roughly of the same magnitude, but of opposite sign. The "most recalcitrant problem" of determining the anharmonic coupling parameters was solved[10] by fitting them to the empirically determined coefficients of a Landau free-energy expansion,[12] thus assuming validity of mean-field theory. The authors[10] themselves are "careful not to assign too much significance to (their) particular anharmonic forces." It was indeed shown by Migoni *et al.*[13] that the anomalously large value of the fourth-order repulsive Ti-O interaction should be attributed to the intraionic anharmonicity that arises from the highly nonlinear polarizability of the oxygen ions. Furthermore, when the third-order repulsive parameter for the Ti-O interaction is determined from static values, either of third-order elastic (TOE) constants, or of the hydrostatic pressure coefficient of the dielectric constant (both obtained by extrapolation of experimental data to absolute zero so as to eliminate thermal and zero-point contributions) values considerably larger than those of Ref. 10 are obtained,[14] thus potentially offsetting the delicate balance between $\Delta^{(3)}$ and $\Delta^{(4)}$.

Clearly, for a more quantitative verification of the theoretical models and for a comprehensive and consistent account of anharmonic properties, more experimental data, also for other compositions, are needed for the determination of the anharmonic parameters. Specifically, for the determination of the *bare* parameters (without thermal and zero-point contributions), data on the temperature dependence of anharmonic properties are required.

The purpose of the present and of a subsequent paper is to present results of accurate measurements of the TOE constants of the fluoroperovskite $KMnF_3$ as a function of temperature, plus some room-temperature data on fourth-order elastic (FOE) constants.

The TOE (and FOE) constants were chosen because (after subtracting the usually smaller Coulomb and the harmonic short-range contributions) they give directly the anharmonic repulsive parameters; and furthermore (since the paraelectric perovskite structure is centrosymmetric) because the deviations from the Cauchy relations give the contributions from noncentral and many-body interactions. The latter are rather large for perovskites as far as data are available.[15–17] $KMnF_3$ was chosen in order to provide empirical input data for a theoretical study of the improper ferroelastic phase transitions at 91.5 and

186 K driven by the softening of the M_3 and R_{25} zone boundary modes, respectively. Specifically, it is intended to investigate the anharmonic forces and their effect on the mode softening without the additional complications in $SrTiO_3$ which arise from the soft Γ_{15} zone center mode and from the unusual nonlinear electronic polarizability of the O^{2-} ion.[13] Furthermore, none of the fluoroperovskites for which the TOE constants are known[16,17] undergoes a phase transition, and comparison with the anharmonic properties of $KMgF_3$ and $KZnF_3$ (Refs. 17 and 18) which do not undergo a phase transition was expected to shed light on the role of the Mn ion in $KMnF_3$ in causing the mode softening.

In this paper we present and discuss experimental results on the pressure derivatives of the second-order elastic constants obtained from ultrasonic velocity measurements. Because of sample brittleness the individual TOE constants could not be measured by application of uniaxial stress. Therefore, the remaining data required for determining the complete set of the six TOE constants were measured separately by means of acoustic harmonic generation and will be reported elsewhere.[19]

The goal of the measurements under hydrostatic pressure was to cover the temperature range above the transition, which is accompanied by an elastic anomaly,[20–22] up to sufficiently high temperature where the temperature dependence is linear, so as to permit linear extrapolation to absolute zero. In the approximation of first-order anharmonic perturbation theory the values obtained in this manner represent *bare* constants, pertaining to the static crystal without thermal and zero-point contributions,[23,24] and also without the effect of the phase transition. This procedure was possible for the first pressure derivatives only, so that for the second pressure derivatives we only report room-temperature values.

II. EXPERIMENTAL DETAILS

A. Sample

The single-crystal boule used in the present work was grown at Cristal Tec., Grenoble, by the Czochralski technique. It is pink and optically transparent; by means of standard stress-optical methods it was ascertained to be stress free. The crystal density is 3.392_5 g/cm^3 at room temperature. Two samples were cut from the boule. Sample 1 is a cube with pairs of parallel faces of (110), $(1\bar{1}0)$, and (001) orientation and normal distances of 1.0688, 1.0394, and 1.0630 cm, respectively. Sample 2 has only one pair of polished (111) faces 0.7559 cm apart; the other two unpolished faces have the orientation $(11\bar{2})$ and $(1\bar{1}0)$ with distances of 1.2 and 0.9 cm, respectively. This sample was only used for second-harmonic generation measurements to be reported elsewhere.[19] The orientation was done by the Laue back-reflection method with an accuracy of 0.3°. The faces were polished by using a Logitec Polishing Machine. With 1-μm diamond paste a flatness better than $\frac{1}{2}\lambda$ sodium light and parallelism of the faces within 0.001° was achieved. All measurements reported here are performed with sample 1.

B. Hydrostatic pressure systems with temperature control

For the hydrostatic measurements, two systems were used in order to extend the available temperature region. One is a small cryogenic pressure vessel made of Be-Cu alloy with a cylindrical internal space 1 in. long and a diameter of 0.6 in.[25] The sample is supported by two soft copper foil springs which are attached to the vessel seal. Pressure in the vessel is generated by an Aminco 46-14021 two-stage compressor with helium gas as pressure medium. The pressure is measured with a calibrated Heise-Bourdon gauge with an accuracy of ± 0.7 bar. The system is capable of generating pressure up to 2 kbar. This pressure vessel can be screwed to a temperature-controlled block of a cryostat. The temperature can be controlled within 0.01 K by adjusting the electric current delivered to the heater through a feedback circuit. For measuring the temperature variation of the sound velocity without applying pressure, the sample is directly in contact with the temperature-controlled block through a sample holder. The temperature was recorded by a Keithley 191 Digital Multimeter through a platinuum-resistance thermometer with an accuracy of 0.01 K.

For measurements above room temperature another pressure vessel was used.[26] It is a Vasco steel cylinder of 37 in. length, 10 in. outside diameter and 2 in. internal diameter. It is equipped with an internal furnace and an outside water jacket. By using a Harwood two-stage compressor a maximum pressure of 10 kbar can be achieved. Temperature control to within 0.05 K is accomplished by adjusting the electric current delivered to the furnace and maintaining constant temperature in the water jacket by circulation water from a thermal bath. Pressure was recorded by a Doric Trendicator 410 A pressure gauge with an accuracy of ± 5 bar. For temperature variation above room temperature without applying pressure, experiments are performed in a simple furnace with a fine-adjustable transformer. The temperature is controlled by adjusting the electric current and the thermal radiation of the furnace. A Chromel-Alumel thermocouple, which is in contact with the sample, gives a temperature resolution of 0.01 K.

C. Ultrasonic interferometer

The pulse-superposition method[25,27] was used to measure the ultrasonic velocities at a frequency of 20 MHz as a function of pressure and temperature. By using an automatic electronic peak finder[25] a precision of better then 10^{-6} was achieved. *X*- and *AC*-cut quartz transducers with diameters of 0.18 in. were used to generate longitudinal and transverse acoustic waves. The bond material was Non-aq stopcock grease (Fisher Scientific Company).

III. EXPERIMENTAL RESULTS FOR $KMnF_3$

A. Temperature dependence of second-order elastic constants

By using the small simple furnace and the low-temperature system, the transit time of the ultrasonic wave in the sample was measured for four different modes as function of temperature. Figure 1 shows the re-

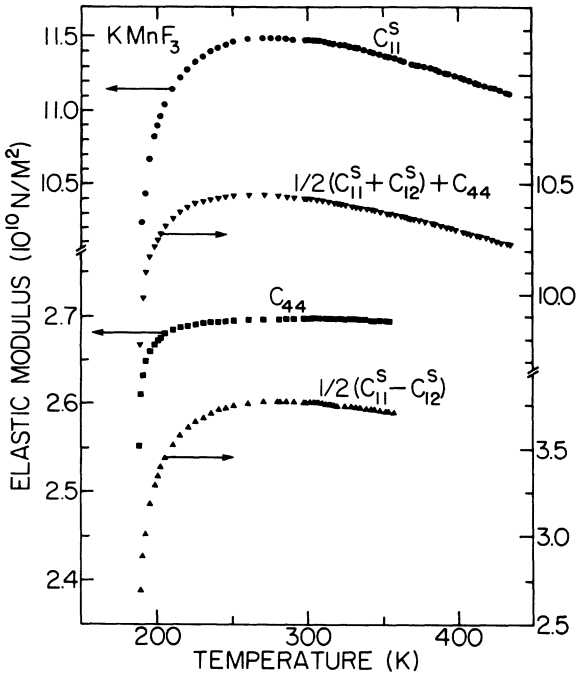

FIG. 1. Elastic constants for directly measured modes vs temperature.

sults of ρv^2 for these modes, where v is the sound velocity at temperature T and ρ the density at the same temperature. ρv^2 is equal to the second-order elastic constants as shown in Fig. 1 for each individual mode.

In order to determine the slope of the elastic constants versus temperature well above the elastic anomaly due to the phase transition, more data points were taken in the high-temperature region. The bond correction is neglected in our calculation since it was found to be insignificant. Data taken in the two systems (below and above room temperature) join smoothly near room temperature although they were taken at different times and with different bonds. In order to avoid breaking the crystal by passing through the phase transition, the minimum temperature was kept about 4 K above T_0 ($\approx$186 K). The two longitudinal modes in [001] and [110], i.e., c_{11}^s and $(c_{11}^s+c_{12}^s)/2+c_{44}$ were measured from 190 to 430 K, but the two transverse modes in these directions, i.e., c_{44} and $(c_{11}^s-c_{12}^s)/2$ were only measured from 190 to 350 K because for this crystal the Non-aq stopcock grease cannot support transverse modes above 360 K. Above 350 K the attenuation of the transverse modes increases strongly and the data are not reliable.

In the high-temperature region ($T \gg T_0$) the elastic constants decrease linearly with temperature for the four directly measured modes. On the other hand, in the low-temperature region near T_0 the curves are bent down when approaching the phase transition from above. At an intermediate temperature ρv^2 reaches a maximum. In [001] the maxima for the longitudinal and transverse modes are at 275 and 285 K, and in [110] at 270 K for the longitudinal mode and 307 K for the transverse mode with polarization along [$1\bar{1}0$], respectively. Figure 1 shows that in the high-temperature limit the transverse modes have smaller temperature coefficients than the longitudinal modes. Although the transverse modes were measured over a relatively smaller temperature range, their linear temperature dependence is well documented. In the high-temperature limit the three independent second-order elastic constants c_{11}^s, c_{12}^s, and c_{44} were fitted to straight lines; the constants defined by the equation

$$c_{\mu\nu}=c_{\mu\nu}^0+A_{\mu\nu}T \tag{3.1}$$

are listed in Table I. $c_{\mu\nu}^0$ are the *bare* constants that are needed as input for lattice dynamic models.

TABLE I. *Bare* values $c_{\mu\nu}^0$ and $\gamma_{\mu\nu}^{(3),0}$, plus high-temperature limit of temperature coefficients $A_{\mu\nu}$ and $B_{\mu\nu}$ of adiabatic second-order elastic constants and partial contractions of isothermal TOE constants, respectively.

	11	12	44
$c_{\mu\nu}^0$ (10^{10} N/m^2)	12.55	4.53	2.71
$A_{\mu\nu}$ (10^7 N/m^2 K)	−3.30	−0.71	−0.04
$\gamma_{\mu\nu}^{(3),0}$ (10^{10} N/m^2)	−165.6	−77.2	−27.2
$B_{\mu\nu}$ (10^8 N/m^2 K)	3.56	10.73	−0.097

The bulk modulus calculated from the four directly measured modes shows only very little temperature variation between 190 and 350 K and passes through a broad maximum of 6.4934×10^{10} N/m^2 at 260 K.

B. First pressure derivatives of elastic constants versus temperature

From 200 to 280 K the measurements under hydrostatic pressure were performed in the small Be-Cu pressure vessel. The data were taken at constant temperature each time after the pressure was reduced from its initial maximum value. It takes 30–40 min for the system to reach thermal equilibrium after each decrement of pressure.

For measurements at and above room temperature, the experiments were performed in the larger vessel with an internal furnace. The main difficulty in the high-temperature measurements is caused by the bond material. Several materials were tried; most of them transmit transverse modes only for temperatures up to 325 K, but longitudinal modes up to 473 K. The best bond material found is a phthalic anhydride ($C_8H_4O_3$) glycerin solution, which transmits both transverse and longitudinal modes up to 413 K under pressure. Data were taken during decreasing pressure and temperature.

If L_0 denotes the length of the unstressed sample at temperature T, and τ the round-trip time of the ultrasonic wave, then the natural velocity is given by $W=2L_0/\tau$. The isothermal first-pressure derivatives $c_0'=(\partial c/\partial p)_{p=0}$ of the adiabatic effective elastic constants can be calculated from the relation[28]

$$c_0'=\rho_0 W_0^2/3B^T+(\rho_0 W^2)'_{p=0}\,. \tag{3.2}$$

Here ρ_0 is the density of the crystal at temperature T without external pressure. Corrections were made for the changes of length and volume at temperatures different

from 298 K.[29]

Figures 2(a) and 2(b) show the isothermal pressure derivatives of the second-order adiabatic elastic constants calculated according to Eq. (3.2) from the measured data of $(\rho W^2)'_{p=0}$. The derivatives also show similar behavior to that of the second-order elastic constants, viz., an anomalous drop near the transition temperature T_0 and linear temperature dependence far above T_0. Among these pressure derivatives $(\partial c_{11}^s/\partial p)_T$ has the strongest temperature dependence; its value changes monotonically from -10.8 at 200 K to 7.23 at 398 K; $(\partial c_{12}^s/\partial p)_T$ decreases with temperature from 9.8 at 200 K to 3.5 at 398 K. $(\partial c_{44}/\partial p)_T$ is weakly temperature dependent and changes sign at about 220 K. In order to illustrate how the slope changes with temperature, one set of the original data of ρW^2 versus pressure is given in Fig. 3 for the longitudinal mode in [001]. Clearly, the slope changes sign with increasing temperature. It is apparent from Figs. 2(a), 2(b), and 3 that in the absence of the phase transition these pressure derivatives would depend linearly on temperature. It should also be mentioned that the longitudinal modes were measured up to 500 K, and that the temperature dependence remains strictly linear.

Four different modes were measured in the hydrostatic experiments. Since for cubic symmetry only three of the modes are independent, a standard least-squares error method[30] was used for the data analysis, and only data points of equal temperature were retained in the final calculations. The error of these pressure derivatives is within 0.3%.

While the pressure derivatives depend on both second- and third-order elastic constants, it is possible to separate these contributions. In this way one obtains the partial contractions $\Gamma^{(3)}_{ijklmn}$ of the TOE constants which are for O_h symmetry given in Voigt notation by[31]

$$\gamma_{11}^{(3)}=c_{111}+2c_{112}\ , \tag{3.3a}$$

$$\gamma_{12}^{(3)}=c_{123}+2c_{112}\ , \tag{3.3b}$$

$$\gamma_{44}^{(3)}=c_{144}+2c_{166}\ . \tag{3.3c}$$

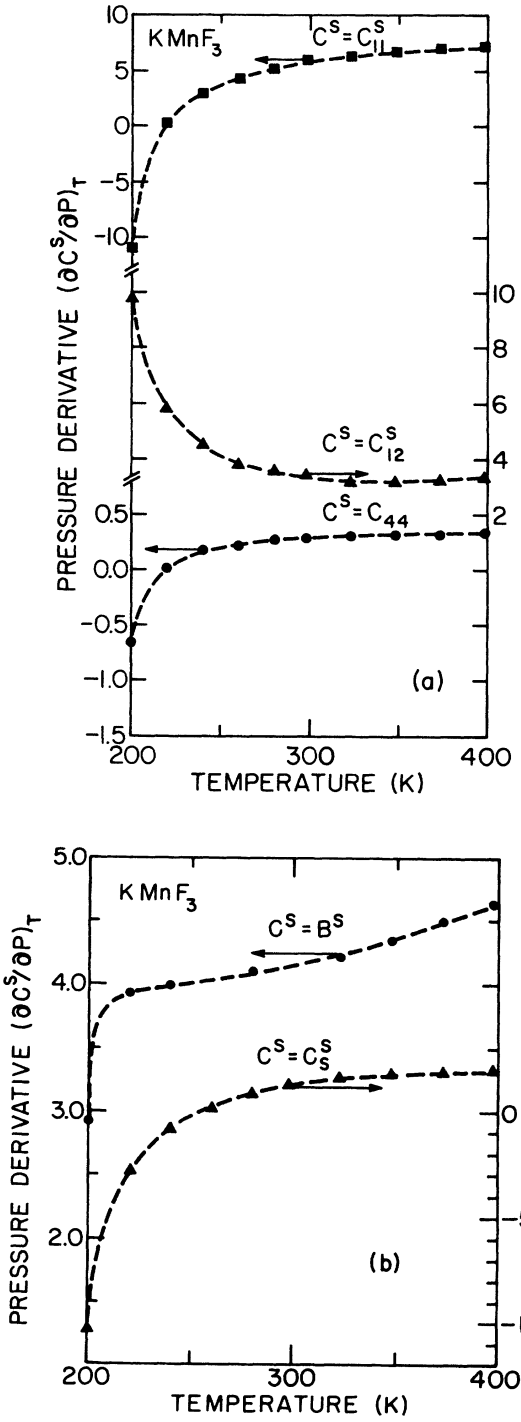

FIG. 2. Pressure derivatives of elastic constants vs temperature, (a) moduli c_{11}^s, c_{12}^s, and c_{44}, (b) shear modulus $c_s=(c_{11}^s-c_{12}^s)/2$ and bulk modulus B^s.

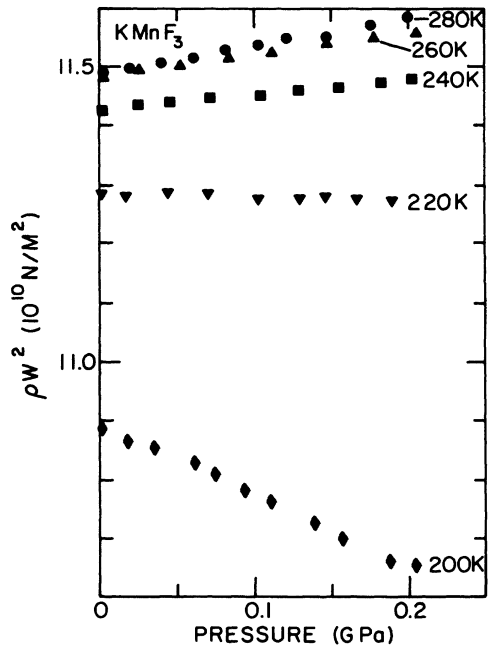

FIG. 3. Pressure dependence of ρW^2 for longitudinal mode in [001] at different temperatures.

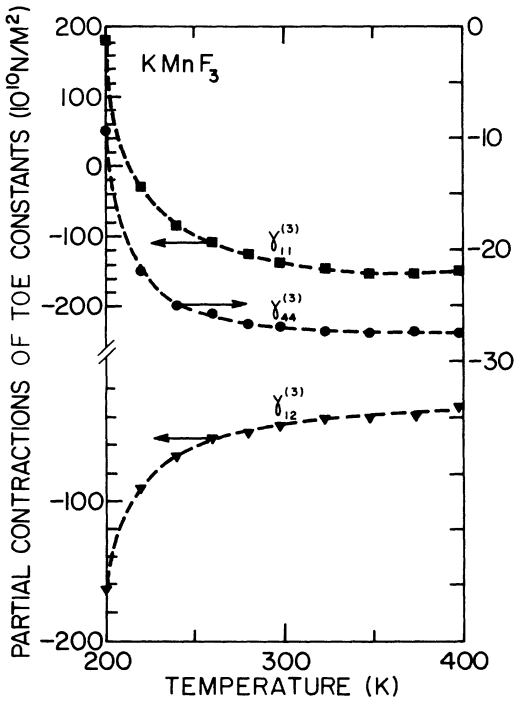

FIG. 4. Partial contractions of isothermal third-order elastic constants vs temperature.

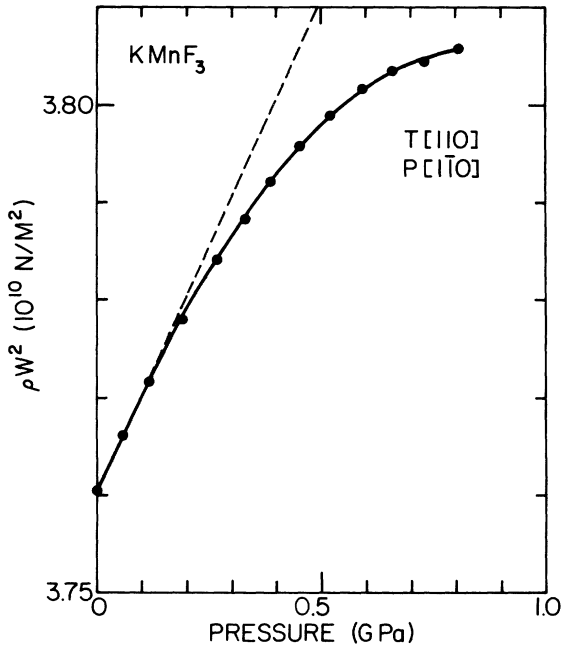

FIG. 5. Pressure dependence of ρW^2 for [110]/[1$\bar{1}$0] transverse mode at 298 K. The solid line represents a quadratic least-squares fit.

They can be calculated from the pressure derivatives according to

$$\gamma_{11}^{(3)} = -\{c_{11}^s + 3B^T[1+(\partial c_{11}^s/\partial p)_T]\} , \quad (3.4a)$$

$$\gamma_{12}^{(3)} = -\{c_{12}^s + 3B^T[(\partial c_{12}^s/\partial p)_T - 1]\} , \quad (3.4b)$$

$$\gamma_{44}^{(3)} = -\{c_{44} + 3B^T[1+(\partial c_{44}/\partial p)_T]\} . \quad (3.4c)$$

Since both the isothermal and adiabatic quantities enter these equations they give the "mixed" contractions. Conversion to purely isothermal contractions[31] gives the data as shown in Fig. 4 versus temperature. The magnitudes of the partial contractions of the TOE constants are over ten times larger than the second-order elastic constants, so that the pressure derivatives are determined by the TOE constants. Figure 4 shows that well above the phase transition in the high-temperature limit the partial contractions of the TOE constants also depend linearly on temperature. Therefore, in order to determine the *bare* partial contractions of TOE constants their temperature dependence was also extrapolated linearly from the high-temperature region. The constants defined in analogy to Eq. (3.1) are also given in Table I.

C. Room-temperature measurements

At room temperature the measurements were carried to higher pressure (8–10 kbar) than at the other temperatures (2–7 kbar). Under such high pressure some curvature can be detected, and a quadratic fit is used in the analysis of the room-temperature data instead of the linear fit at other temperatures. Figure 5 shows as a typical set of experimental data the [110]/[1$\bar{1}$0] transverse mode. These data can be well fitted to a parabola (solid line).

The second pressure derivatives of the elastic constants can be calculated from the equation[28]

$$c_0'' = \rho_0 W_0^2 L_0'' + 2(\rho_0 W^2)_0' L_0' + (\rho_0 W^2)_0'' . \quad (3.5)$$

The quantities L_0' and L_0'' take into account the pressure-induced dimensional change of the sample and for cubic symmetry can be expressed in terms of the bulk modulus B and its first pressure derivative.[28]

In Table II the room-temperature (298 K) values of the isothermal and adiabatic second-order elastic constants are listed. These values were obtained by extrapolating the pressure data to zero pressure by means of a quadra-

TABLE II. Adiabatic and isothermal second-order elastic constants (in 10^{10} N/m^2) at 298 K.

	c_{11}	c_{12}	c_{44}	c_S	B
Adiabatic	11.480	3.956	2.6989	3.7603	6.463
	±0.004	±0.004	±0.0001	±0.0003	±0.004
Isothermal	11.281	3.761	2.6989	3.7603	6.268
	±0.004	±0.004	±0.0001	±0.0003	±0.004

TABLE III. Adiabatic, isothermal, and mixed first pressure derivatives of the second-order elastic constants at 298 K.

	$\partial c_{11}/\partial p$	$\partial c_{12}/\partial p$	$\partial c_{44}/\partial p$	$\partial c_S/\partial p$	$\partial B/\partial p$
$(\partial c^S/\partial p)_S$	5.929	3.370	0.280	1.279	4.220
	±0.014	±0.014	±0.005	±0.014	±0.014
$(\partial c^S/\partial p)_T$	5.929	3.399	0.281	1.265	4.242
	±0.014	±0.014	±0.005	±0.014	±0.014
$(\partial c^T/\partial p)_T$	5.822	3.292	0.281	1.265	4.136
	±0.014	±0.014	±0.005	±0.014	±0.014

tic least-squares fit. The extrapolated values agree with those from measurements of the temperature dependence at zero pressure within 0.05%. The discrepancy is attributed to the fact that different electronic equipment was used for the two sets of measurements.

By using Eqs. (3.2) and (3.5) the first and second pressure derivatives of c_{11}^s, c_{12}^s, and c_{44} were determined; the former are given in Table III together with the purely isothermal and adiabatic quantities $(\partial c^s/\partial p)_s$ and $(\partial c^T/\partial p)_T$. The specific heat c_p used for the conversion between isothermal and adiabatic quantities was calculated according to the Debye approximation by using the elastic Debye temperature. Table IV lists the second pressure derivatives of the second-order elastic constants at room temperature. From these quantities one can calculate the partial contractions $\Gamma^{(4)}_{ijklmnn}$ of the fourth-order elastic constants given by[32]

$$\gamma_{11}^{(4)}=c_{1111}+4c_{1112}+2c_{1122}+2c_{1123}\ , \tag{3.6a}$$

$$\gamma_{12}^{(4)}=2c_{1112}+2c_{1122}+5c_{1123}\ , \tag{3.6b}$$

$$\gamma_{44}^{(4)}=c_{1144}+2c_{1166}+4c_{1244}+2c_{1266}\ . \tag{3.6c}$$

In Table V these mixed partial contractions are listed together with the isothermal partial contractions of the TOE constants. The latter are about 330, 840, and 30 times larger than the respective second-order elastic constants. Since for cesium halides the partial contractions of the fourth-order elastic constants are only about 100 times larger than the second-order elastic constants,[33] this indicates unusually large (small) fourth-order anharmonicity for c_{12} (c_{44}), respectively. Large derivations from the Cauchy relations $\gamma_{12}^{(3)}=\gamma_{44}^{(3)}$ and $\gamma_{12}^{(4)}=\gamma_{44}^{(4)}$ occur, especially for the fourth-order elastic constants, indicating unusually strong many-body contributions to the latter.

D. Experimental errors

All experimental errors shown in Tables II–IV are standard errors from simultaneous least-squares fits of three independent elastic constants and their (first and second) pressure derivatives to the four different acoustic modes measured as functions of pressure. They are mostly due to sample inhomogeneities and misalignment of the crystal surfaces. Additional systematic errors arise from measurement of sample dimensions, density, travel time, and pressure. These errors are estimated as 0.1% 1%, and 2% for the elastic constants, and for their first and second pressure derivatives, respectively.

IV. DISCUSSION

A. Second-order elastic constants

The three second-order elastic constants of $KMnF_3$ have been measured before with an ultrasonic pulse method at 30 MHz from 200 K to room temperature by Alexandrov, Reshchikova, and Beznosikov[20] (ARB), and c_{11} has been measured by a continuous wave resonance technique at 5 MHz from 120 to 370 K by Melcher and Plovnick[21] (MP). Since the data show very little scatter they are shown as smooth curves in Fig. 6 together with our present results.

The most conspicuous feature is the cusplike anomaly around the transition temperature T_0. This anomaly has also been studied for other perovskites ABX_3, especially in the critical regime close to and above T_0 (see, e.g., Refs. 34–36 and references therein). It has been attributed to fluctuations of the order parameter (the rotation angles of the BX_6 octahedra) and should for $T>T_0$ decay as $(T-T_0)^{-\delta}$ (Refs. 36–39). Above the critical regime δ is not a universal critical exponent and not well known theoretically. In the context of the present paper the acoustic anomaly is of interest mostly because it is needed to determine its width and to identify the temperature above which the effect of the fluctuations has subsided so as to permit determination of the *bare* elastic constants by linear extrapolation to $T=0$. Whereas in $SrTiO_3$ the anomaly is quite narrow [about 10 K for 10^7–10^8 Hz (Refs. 34 and 38)], according to Fig. 6 it is much wider

TABLE IV. Second pressure derivatives of second-order elastic constants (in 10^{-10} m^2/N) at 298 K.

	$\partial^2 c_{11}/\partial p^2$	$\partial^2 c_{12}/\partial p^2$	$\partial^2 c_{44}/\partial p^2$	$\partial^2 c_S/\partial p^2$	$\partial^2 B/\partial p^2$
$(\partial^2 c^S/\partial p^2)_T$	−17.3	7.0	−0.8	−12.2	−1.1
	±2.7	±2.8	±0.1	±0.4	±2.7

TABLE V. Isothermal and mixed partial contractions of third- and fourth-order elastic constants, respectively (in 10^{10} N/m^2) at 298 K.

$\mu\nu$	11	12	44
$\gamma_{\mu\nu}^{(3)}$	-140.3 ± 3	-47.6 ± 3	-26.8 ± 0.1
$\gamma_{\mu\nu}^{(4)}$	-3900 ± 1000	3300 ± 1000	84 ± 40

for $KMnF_3$, almost 150 K. This is a consequence of the weak dispersion of the soft zone boundary modes between the R and M points[40] which restricts the fluctuations to the $\{100\}$ planes and drives the transition weakly first order.[41]

Although the elastic anomaly observed by MP and by us is in qualitative agreement their anomaly is narrower than ours, and their linear high-temperature regime starts at a lower temperature (about 300 K) than ours (about 350 K). Furthermore, the data of MP are larger than ours (about 2%) in the high-temperature regime. These discrepancies could possibly arise from sample differences and/or from the different experimental techniques and frequencies used.

The aspect most important for the purposes of the present paper is *the existence of a linear high-temperature regime for* c_{11} in the data of MP, and *the close agreement of their slope with that of our data.*

The data by ARB for c_{11} do not show a maximum, but an increase in slope around 275 K. However, all three curves of ARB are (except for the two data points for c_{11} at 275 and 295 K) congruent with the curves based on our data, but are shifted to higher temperature by about 10 K; furthermore, ARB's data for c_{44} are 1% larger than ours. In this context is should be noted that the transition temperature of our sample was 186 K, in agreement with virtually all of the large number of papers on $KMnF_3$, but that ARB report a transition temperature of 198 K for their sample.[20] However, by shifting their curves by about 10 K to lower temperature they can be brought into coincidence with ours (except for the two data points for c_{11} at 275 and 295 K, and the aforementioned shift in c_{44}). Thus, if one assumes that the temperature scale of ARB below room temperature is subject to a systematic error of about 10 K, the discrepancy between their and our data, and especially between the opposite signs of the temperature coefficient for c_{11}, is resolved: then c_{11} reaches its maximum value at room temperature, and the upper limit of the fluctuation regime (about 350 K) was not reached by ARB. Since both their and our measurements were made with ultrasonic pulse methods at comparable frequencies we suggest, subject to confirmation by extension of the measurement on ARB's sample to higher temperature, that the crystals used in these two experiments were of comparable quality and composition, and that above 200 K the acoustic anomaly is an intrinsic effect.

Finally, we note that in the low-temperature phase ($T < 186$ K) there is a pronounced difference between the data for c_{11} of MP and ARB. This can most likely be attributed to different domain configurations in the two samples used, resulting from differences in sample size and geometry, as well as defect content, and to some extent to the fact that these data were taken at different frequencies and by different methods.

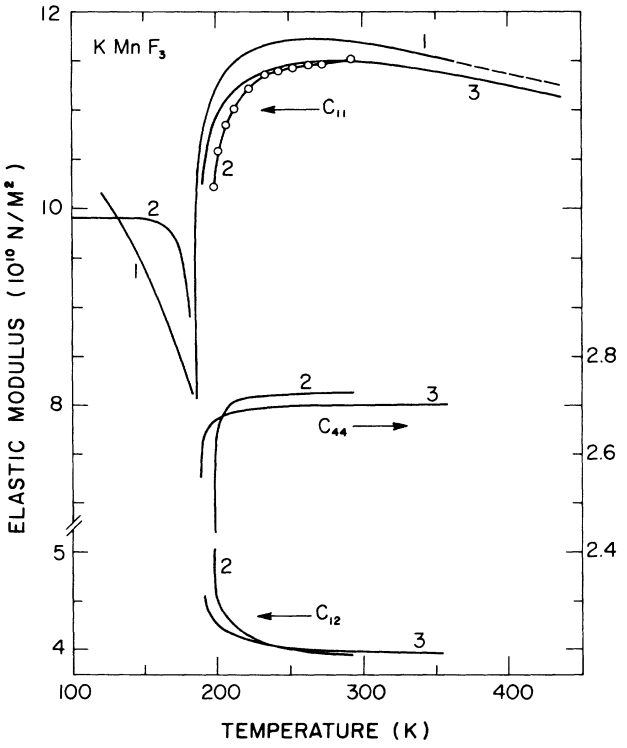

FIG. 6. Comparison of elastic-constant data by different authors with results from present work. [1, Melcher and Plovnick (Ref. 21); 2, Alexandrov *et al.* (Ref. 20); 3, present work].

B. Grüneisen parameters

The thermal Grüneisen parameter

$$\gamma^{\text{th}} = \beta B^T / \rho c_p \tag{4.1}$$

(β is the volume thermal expansion coefficient, B^T is the isothermal bulk modulus, ρ is the density, c_p is the specific heat) is in the quasiharmonic approximation given by the mode average[42]

$$\gamma = \sum_i c_i^{\text{th}} \gamma_i \Big/ \sum_i c_i^{\text{th}} . \tag{4.2}$$

Here c_i^{th} denotes the Einstein specific heat and γ_i the microscopic Grüneisen parameter (mode gamma)

$$\gamma_i = -(V/\omega_i)(\partial\omega_i/\partial V)_T \tag{4.3}$$

of the ith vibrational mode, respectively, and V the volume.

Although the mode average (4.2) depends on both the anisotropy and the dispersion of the γ_i, for many materials surprisingly good agreement with γ^{th} is obtained by evaluating (4.2) in the long wave length acoustic limit (anisotropic elastic continuum approximation[43]), i.e., in these cases the average (4.2) is determined primarily by

the anisotropy. Discrepancies between γ^{th} and γ^{el} (evaluated in this manner), when they occur, give indirect information on the dispersion of γ_i. Application of this procedure to $KMnF_3$ is of interest because it allows one to verify the existence of a cutoff frequency $1/\tau$ for the fluctuation contribution to the elastic constants and their pressure derivatives. $\tau=2\Gamma/\omega_R^2$ is the relaxation time[37,38] of the soft R_{25} mode (with frequency ω_R and linewidth Γ) and marks the transition from the hydrodynamic (fluctuation) regime $\omega\tau<1$ to the ballistic regime $\omega\tau>1$.

Comparison of Figs. 1 and 2 shows that the shape and width of the acoustic anomalies for the elastic constants and their pressure derivatives are rather similar; this implies that their frequency dependence and, specifically, the cutoff frequencies should also be similar.

In the anisotropic elastic continuum approximation the mode γ's are determined by the second-order elastic constants and their first pressure derivatives. For cubic symmetry it is[43]

$$\gamma_i=(B^T/2c_i)(\partial c_i/\partial p)_T-\tfrac{1}{6}\ . \tag{4.4}$$

Here $c_i=\rho V^2$ is the effective elastic constant pertaining to a particular mode for a given direction.

In Figures 7(a) and 7(b) the three elastic mode γ's (4.4) are plotted versus direction at room temperature and at 200 K, respectively. While the anisotropy of the elastic constants is small and independent of temperature, the mode γ's depend strongly on direction and temperature. At room temperature γ_1 has a minimum near [111], γ_2 and γ_3 have maxima in [110] and near [111], respectively. At 200 K all extrema occurring at room temperature are reversed. At room temperature all three mode γ's are positive, but become negative at 200 K for almost all directions.

Figures 7(a) and 7(b) were calculated from the ultrasonically measured elastic data which include the fluctuation contribution. On the other hand, the corresponding curves for the high-frequency regime $\omega>1/\tau$, obtained by subtracting the fluctuation contribution from the elastic data in the manner described above, are qualitatively and semiquantitatively very similar to the room temperature curves [Fig. 7(a)] and depend only weakly on temperature.

The thermal Grüneisen parameter was calculated from experimental thermal-expansion data[29] and by using the Debye approximation for the specific heat with $\Theta_D=470.1$ K (396.8 K) for $T=298$ K (200 K), respectively, calculated from the measured temperature-dependent elastic constants. Also shown in Fig. 8 are the elastic γ's γ_H^{el} and γ_L^{el}, calculated according to (4.2) in the anisotropic continuum approximation for the high- and low-frequency limits $\omega\tau\gg1$ (H) and $\omega\tau\ll1$ (L), respectively, both evaluated in the high- and low-temperature limits ($T\geq\Theta_D$, denoted by ∞; and $T=0$, denoted by 0, respectively).

It is apparent that $\gamma_{L,\infty}^{el}$ and $\gamma_{L,0}^{el}$ decrease strongly and become negative at lower temperature, reflecting the effect of fluctuations on $(\partial c_{\mu\nu}/\partial p)$, but do not differ much from each other. On the other hand $\gamma_{H,\infty}^{el}$ and

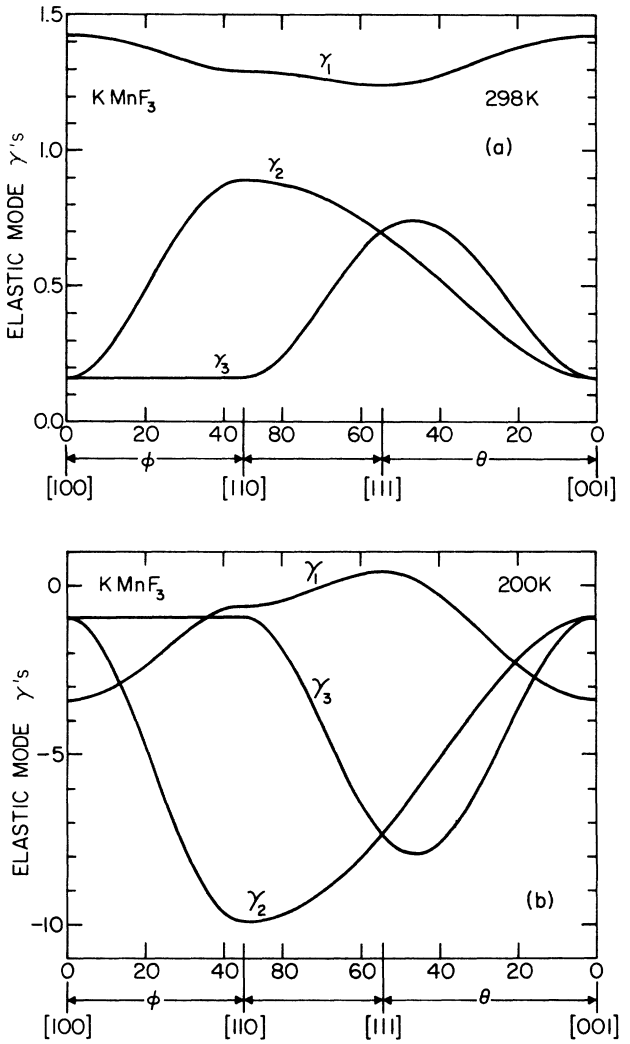

FIG. 7. Elastic-mode γ's vs direction. θ and ϕ are the polar angles (in degrees) of the wave vector with the polar axis in [001]. (a) 298 K, (b) 200 K.

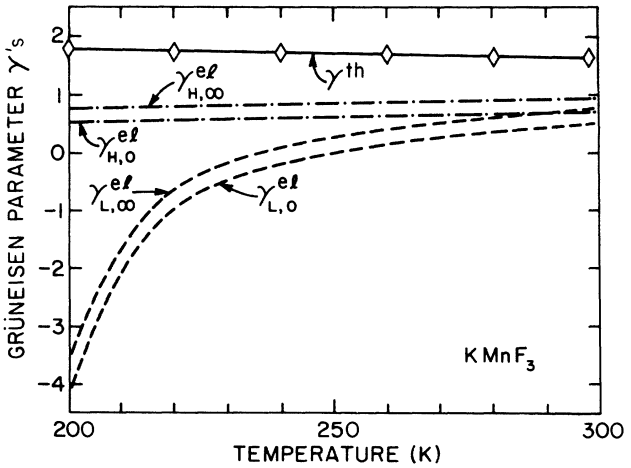

FIG. 8. Elastic (el) and thermal (th) Grüneisen parameters vs temperature. The subscripts H and L refer to the low- and high-frequency limits, and the subscripts 0 and ∞ refer to the low- and high-temperature limits of the mode average according to Eq. (4.2), respectively.

$\gamma_{H,0}^{el}$, because of the absence of the fluctuation contribution, decrease only slightly with decreasing temperature, and also differ only a little from each other. γ^{th} increases weakly with decreasing temperature. The weak-temperature variation of γ_H^{el} corresponds to that of γ^{th}; however, a discrepancy by an almost constant factor of about 2 is apparent and may be attributed to the neglect of dispersion and of optic-mode contributions in the anisotropic elastic continuum model.

The temperature dependence of γ_L^{el} disagrees qualitatively with that of γ^{th}. This can be understood in terms of the volume fraction f in phase space in which the contribution from the fluctuation-dominated acoustic mode γ's should be significant. In the Debye approximation one obtains $f=(\omega_D\tau)^{-3}$, where $\omega_D=$ Debye frequency. From the linewidth and frequency of the soft R_{25} mode determined for $KMnF_3$ at 295 K by inelastic neutron scattering[40] one obtains $f=2.25\times10^{-4}$. Since τ increases with decreasing temperature, f decreases even further as the transition temperature is approached.

C. Short-range parameters

In the rigid shell model the second- and higher-order elastic constants are for centrosymmetric cubic perovskite materials ABX_3 additively composed of Coulomb and (repulsive) short-range contributions, where the former depend only on the effective ionic charges Z_A, Z_B, and Z_X, but not on the electronic polarizabilities of the ions.[44,14] Taking for the charges in $KMnF_3$ (and the other fluoroperovskites to be considered here) the free-ion values[45] $+1$, $+2$, and -1, respectively, and assuming short-range central-force pair-potential interactions $\varphi_\beta(r_\beta)$ between nearest-neighbor ions (with $\beta=1$, 2, 3 denoting A-B, B-X, and X-X interactions, respectively) we can therefore calculate the first- through fourth-order derivatives of the pair potential from the equilibrium condition ($p=0$) and from our experimental values of the second-order elastic constants and of the partial contractions of the TOE and FOE constants. Since the latter could only be measured at room temperature we restrict ourselves here to an approximate analysis based on room-temperature input data.

In the Appendix the equilibrium condition, the second-order elastic constants (based on expressions given by Cowley[44]), and the partial contractions $\gamma_{\mu\nu}^{(3)}$ and $\gamma_{\mu\nu}^{(4)}$ are given for the rigid shell model of Stirling[11] which includes the above three types of short-range interactions. The latter are expressed in terms of the dimensionless derivatives of the pair potentials defined as follows[44,14] [$\beta=1,2,3$]:

$$(e^2/2a^3)B_\beta=(1/r_\beta)(\partial\varphi_\beta/\partial r_\beta)\ , \tag{4.5a}$$

$$(e^2/2a^3)A_\beta=(\partial^2\varphi_\beta/\partial r_\beta^2)\ , \tag{4.5b}$$

$$(e^2/2a^3)C_\beta=r_\beta(\partial^3\varphi_\beta/\partial r_\beta^3)\ , \tag{4.5c}$$

$$(e^2/2a^3)D_\beta=r_\beta^2(\partial^4\varphi_\beta/r_\beta^4)\ . \tag{4.5d}$$

Here a denotes the lattice constant, e the electronic charge, and $r_1=r_3=a/\sqrt{2}$, $r_2=a/2$ the nearest-neighbor distances.

It is apparent from Eqs. (A2), (A3), and (A6) that the K-F and F-F interactions enter the equations only in the additive form (B_1+B_3), (A_1+A_3), etc., and therefore cannot be determined separately. Thus these equations represent seven equations for the eight unknown quantities (B_1+B_2), B_2; (A_1+A_2), A_2; (C_1+C_3), C_2; (D_1+D_3), D_2. In order to get one additional condition the K-F and F-F interactions were calculated from the Huggins-Mayer form $\varphi_\beta(r_\beta)=b_\beta\exp(-r_\beta/\rho)$ ($\beta=1$, 3), with b_β and ρ determined empirically from alkali halides.[46] Having determined (B_1+B_3) in this manner, B_2 was then determined from the equilibrium condition, and the remaining six (combinations of) repulsive parameters were determined from the experimental elastic data c_{11}, c_{12}; $\gamma_{11}^{(3)}$, $\gamma_{12}^{(3)}$; $\gamma_{11}^{(4)}$, $\gamma_{12}^{(4)}$. In addition, the second- and higher-order coupling parameters (A_1+A_3), (C_1+C_3), and (D_1+D_3) were also calculated from the Huggins-Mayer potential. All results are listed in Table VI. For comparison the corresponding coupling parameters up to third order are also listed for $KMgF_3$ and $KZnF_3$, which do not undergo a structural transition, and for which only the first pressure derivatives of the elastic constants are available.[16,18]

The data in Table VI show the following. (i) For the K-F plus F-F interaction the experimental values agree quite well with the calculated harmonic coefficients A_1+A_3, but are about two times and twenty times larger for the anharmonic coefficients C_1+C_3 and D_1+D_3, respectively. This suggests that the (smaller) first derivatives B_1 and B_3 are adequate for the determination of B_2 from the equilibrium condition. (ii) The first and second derivatives (B_2 and A_2) of the (Mg, Zn, Mn)-F interactions are about ten times larger than the combined K-F and F-F interactions, but for the third derivatives this ratio drops to about 2 to 5, and the fourth derivative (D_2) even shows the opposite sign and is numerically four times larger than D_1+D_3. (iii) The details of the calculation (not included in Table VI) show that to all orders the calculated K-F interaction is about twice as large as the F-F interaction. (iv) All first and second derivatives are very similar for the three fluoroperovskites compared in Table VI, but for $KMnF_3$, C_2 is only half as large as for the other two compounds.

The large derivations from the Cauchy relations $\gamma_{12}^{(n)}=\gamma_{44}^{(n)}$ for $n=3$ and, especially for $n=4$ (Table V) have already been noted above, but by themselves they do not provide any clues as to whether noncentral contributions are more pronounced for c_{12} or c_{44} (and their pressure derivatives). In order to decide this question we have repeated the entire determination of the short-range parameters with c_{44}, $\gamma_{44}^{(3)}$, and $\gamma_{44}^{(4)}$ as experimental input (instead of c_{12}, $\gamma_{12}^{(3)}$, and $\gamma_{12}^{(4)}$). Surprisingly, there are few drastic changes in the repulsive parameters, except that for the K-F plus F-F interaction the agreement between calculated and experimental values was less satisfactory, and that a 50-% smaller value was obtained for D_2. In addition, since the experimental error of $(\partial^2 c_s/\partial p^2)$ is smaller than for the other second pressure derivatives used as input (see Table IV), we have repeated the parameter determination with c_s and its pressure derivatives as

TABLE VI. Short range coupling parameters for three fluoroperovskites derived from room-temperature elastic data. Data in parentheses are calculated from Huggins-Mayer model (Ref. 46).

	$KMgF_3$	$KZnF_3$	$KMnF_3$
Lattice Constant (nm)	0.3989	0.4055	0.4190
Ref. Elastic data	18	47,16	Present work
B_1+B_3	(−1.65)	(−1.48)	(−1.19)
B_2	−9.92	−10.58	−11.73
A_1+A_3	9.48	15.13	10.46
	(13.74)	(12.57)	(11.71)
A_2	94.62	85.01	89.79
C_1+C_3	−149	−204	−190
	(−115)	(−107)	(−92)
C_2	−701	−760	−348
D_1+D_3			16 700
			(803)
D_2			−59 900

input. Again, the results are quite similar, the largest difference to emerge being a reduction of D_2 from −59 900 to −44 200.

In summary, the most noteworthy result is the relatively small third, and the unusually large fourth derivative of the Mn-F interaction (C_2 and D_2, respectively). Most likely this may be attributed to the partly filled $3d$ shell of Mn, whereas Mg^{2+} and Zn^{2+} have, of course, closed-shell configurations. On the other hand, it is not possible to attribute the R_{25} mode instability in ABF_3 perovskites to some particular electronic configuration of the B ion, because $RbMnF_3$ does not show R_{25}-mode softening,[48] whereas $RbCaF_3$ does.[49]

D. Relation to structural transition

It has been suggested[7,50] that the R_{25}-mode phase transition in ABX_3 perovskites occurs when the B ions are sufficiently "large" so as to reduce the A-X interaction and allow the BX_6 octahedra to rotate more easily. On the basis of this picture one would expect the B-X interaction to increase in the sequence Mg-F, Zn-F, either absolutely, or relative to the K-F interaction. However, according to Table VI this is not the case for the coupling parameters of first, second, and third order. On the contrary, C_2 for $KMnF_3$ is only half the value for $KMgF_3$ and $KZnF_3$. Only the fourth-order coupling parameters are anomalously large, both for the K-F plus F-F, and for the Mn-F interactions. (Unfortunately, for $KMgF_3$ and $KZnF_3$ no data are available for comparison.) It seems implausible to attribute the anomalously large value of D_2 (and D_1+D_3) to an ionic ratio effect or, equivalently, to the range of Hartree-Fock-type wave functions, because in this case the lower-order coupling parameters would be affected too. The situation for $KMnF_3$ is somewhat analogous to that in $SrTiO_3$ where it is also the fourth order, but not the third-order coupling parameters for the Ti-O interaction that are anomalously large.[10] This has been attributed to the nonlinear electronic polarizability of the O^{2-} ions;[13] however, this explanation cannot be expected to be valid for the F ion in $KMnF_3$, because, unlike the O^{2-} ion, it does not require a Watson sphere for stabilization.[51] An alternative explanation would be a charge-transfer mechanism between the Mn and F ions, that could at the same time also account for large many-body effects.[52,53] Conceivably, this feature could also be a manifestation of strongly anharmonic F-F interactions associated with a double-well potential originally proposed[54] for $RbCaF_3$ to account for strong anharmonicity observed in the Debye-Waller factor and more recently found to be consistent with experimental evidence for precursor order close to the transition temperature.[55]

V. SUMMARY AND CONCLUSIONS

The single-crystal elastic constants and their first pressure derivatives have been measured for $KMnF_3$ by means of the ultrasonic pulse superposition method at 20 MHz from 200 to 430 K. At room temperature the second pressure derivatives have also been measured. The salient features of the results and their analysis are as follows.

(i) A downward cusplike anomaly is observed at the improper ferroelastic transition temperature $T_0=186$ K, both for the elastic constants and their pressure derivatives, which extends upward to about 350 K.

(ii) Above 350 K the elastic constants and their pressure derivatives exhibit the usual linear temperature dependence which in the absence of phase transitions is characteristic of the high-temperature regime ($T\geq\Theta_D$) and which permits linear extrapolation to $T=0$ for the determination of the *bare* elastic quantities (without thermal and zero-point motion).

(iii) Analysis of the room-temperature data on the basis of a rigid shell model with nearest-neighbor central-force short-range interactions between K-F, Mn-F, and F-F ions shows that the harmonic contribution from the short-range Mn-F interaction dominates, but that the anharmonic contributions are comparable to the K-F plus F-F interactions, and that especially the fourth-order anharmonic contributions from all three interactions are anomalously large. Furthermore, the anharmonic interactions contain large many-body contributions and are

highly anisotropic.

(iv) The elastic anomaly has been attributed previously to coupling between strain and fluctuations of the order parameter of the 186 K phase transition.[37,38] We find that the small temperature variation of the thermal Grüneisen parameter agrees with that of the elastic Grüneisen parameter without the fluctuation contribution, calculated in the anisotropic continuum approximation by linear extrapolation of our elastic data from the high-temperature regime, but that the elastic Grüneisen parameter with the fluctuation contribution included exhibits the wrong temperature dependence. This is consistent with previous theoretical models[37,38] which indicate that the fluctuation-controlled regime is limited to acoustic frequencies less than the relaxation rate of the soft R_{25} mode.

In a subsequent paper we plan to supplement our present results by measurements of acoustic second-harmonic generation in the high-temperature linear regime.[19] This will permit the determination of the complete set of the *bare* TOE constants for the static crystal to be used as input for a more consistent theory of anharmonic properties and mode softening in $KMnF_3$.

ACKNOWLEDGMENTS

We thank Dr. Z. P. Chang for making available to us his computer program for the least-squares analysis of the experimental data. Ongoing discussions with Dr. B. N. N. Achar and Dr. L. E. Cross on perovskites in general are also gratefully acknowledged. This work was supported by the U. S. Office of Naval Research under Contract No. N00014-82-K-0339.

APPENDIX

In the following we give the equations that were used for the determination of the repulsive parameters in Sec. IV B, viz., the equilibrium condition, expressions for the second-order elastic constants and for the partial contractions of the TOE and FOE constants.

For the cubic perovskite structure pertaining to the composition ABX_3 with Coulomb interactions between the ions with charges $Z_A=1$, $Z_B=2$, and $Z_x=-1$, and with short-range central-force interactions $\varphi_\beta(r_\beta)$, ($\beta=1$, 2, 3) between A-X, B-X, and X-X nearest neighbors, respectively, the lattice energy per formula unit is given by

$$\phi=-\alpha e^2/a+12\varphi_1(r_1)+6\varphi_2(r_2)+12\varphi_3(r_3)\ . \quad \text{(A1)}$$

Here $\alpha=12.377\,468$ denotes the Madelung constant for the above choice of charges,[56] a denote the lattice constant, and r_1, r_2, and r_3 denotes the three types of nearest-neighbor distances as given in Sec. IV C. Writing the derivatives of the pair potentials $\varphi_\beta(r_\beta)$ in the dimensionless form as in Eqs. (4.5a)–(4.5d), the equilibrium condition $[p=-(1/3a^2)(\partial\phi/\partial a)=0]$ becomes[44]

$$4\alpha+12(B_1+B_3)+3B_2=0\ . \quad \text{(A2)}$$

Writing Cowley's expressions for the second-order elastic constants[44] in the form ($\mu\nu=11$, 12, 44)

$$c_{\mu\nu}=(e^2/a^4)\{\sigma^{(2)}_{\mu\nu}+\rho^{(2)}_{\mu\nu}/4\} \quad \text{(A3)}$$

the partial contractions of TOE and FOE constants obtained via proper differentiation[31,32] can be written in the analog form (with $n=3$ and 4, respectively)

$$\gamma^{(n)}_{\mu\nu}=(e^2/a^4)\{\sigma^{(n)}_{\mu\nu}+\rho^{(n)}_{\mu\nu}/4\}\ . \quad \text{(A4)}$$

Here

$$\sigma^{(2)}_{11}=-16.495\,904\ , \quad \text{(A5a)}$$

$$\sigma^{(2)}_{12}=2.059\,218\ , \quad \text{(A5b)}$$

$$\sigma^{(3)}_{\mu\nu}=-5\sigma^{(2)}_{\mu\nu}\ , \quad \text{(A5c)}$$

$$\sigma^{(4)}_{\mu\nu}=35\sigma^{(2)}_{\mu\nu}\ . \quad \text{(A5d)}$$

$\rho^{(n)}_{\mu\nu}$ represent the short-range repulsive contributions; the six independent linear combinations occurring in (A3) and (A4) are

$$\rho^{(2)}_{11}=2\rho^{(2)}_{12}-B_2+A_2\ , \quad \text{(A6a)}$$

$$\rho^{(2)}_{12}=-(B_1+B_3)+(A_1+A_3)\ , \quad \text{(A6b)}$$

$$\rho^{(3)}_{11}=2\rho^{(3)}_{12}+3B_2-3A_2+C_2\ , \quad \text{(A6c)}$$

$$\rho^{(3)}_{12}=3(B_1+B_3)-3(A_1+A_3)+(C_1+C_3)\ , \quad \text{(A6d)}$$

$$\rho^{(4)}_{11}=2\rho^{(4)}_{12}-15B_2+15A_2-6C_2+D_2\ , \quad \text{(A6e)}$$

$$\rho^{(4)}_{12}=-15(B_1+B_3)+15(A_1+A_3)-6(C_1+C_3)+D_1+D_3\ . \quad \text{(A6f)}$$

In Eqs. (A4)–(A6) a redundant factor of 2 has been deleted from Cowley's expressions,[44] and the more accurate values of Naimon[56] are given instead. Furthermore, the equilibrium condition has been used in reducing the repulsive contributions to the form given in Eqs. (A6); this results in the Cauchy relations for $n=2,3,4$:

$$\sigma^{(n)}_{12}=\sigma^{(n)}_{44}\ , \quad \text{(A7a)}$$

$$\rho^{(n)}_{12}=\rho^{(n)}_{44}\ . \quad \text{(A7b)}$$

The Coulomb coefficients satisfy the relations (given in part by Naimon[56])

$$\sigma^{(2)}_{11}+2\sigma^{(2)}_{12}=-\alpha\ , \quad \text{(A8a)}$$

$$\sigma^{(3)}_{11}+2\sigma^{(3)}_{12}=5\alpha\ , \quad \text{(A8b)}$$

$$\sigma^{(4)}_{11}+2\sigma^{(4)}_{12}=-35\alpha\ . \quad \text{(A8c)}$$

[1] B. Wul and I. M. Goldman, C. R. (Dokl.) Acad. Sci. URSS **46**, 139 (1945); **49**, 177 (1945); **51**, 21 (1946).

[2] P. W. Anderson, in *Fizika Dielektrikov*, edited by G. I. Skanavi (Akad. Nauk. SSSR, Moscow, 1959), p. 290.

[3] W. Cochran, Adv. Phys. **9**, 387 (1960).

[4] M. E. Lines and A. M. Glass, *Principles and Applications of Ferroelectrics and Related Materials* (Clarendon, Oxford, 1977).

[5]*Landolt-Börnstein, Numerical Data and Functional Relationships in Science and Technology,* edited by K. H. Hellwege, Group III, Crystal and Solid State Physics, Vol. 16, Ferroelectrics and Related Substances, Subvolume a: Oxides, and Subvolume b: Non-oxides (Springer, Berlin, 1981).
[6]J. F. Scott, Rev. Mod. Phys. **46**, 83 (1974).
[7]A. D. Bruce and R. A. Cowley, *Structural Phase Transitions* (Taylor and Francis, London, 1981).
[8]A. Bednorz and K. A. Müller, Z. Phys. B **64**, 189 (1986).
[9]M. K. Wu, J. R. Ashburn, C. J. Torng, P. H. Hor, R. L. Meng, L. Gao, Z. J. Huang, X. Q. Wang, and C. W. Chu, Phys. Rev. Lett. **58**, 908 (1987).
[10]A. D. Bruce and R. A. Cowley, J. Phys. C **6**, 2422 (1973).
[11]W. G. Stirling, J. Phys. C **5**, 2711 (1972).
[12]J. C. Slonczewski and H. Thomas, Phys. Rev. B **1**, 3599 (1970).
[13]R. Migoni, H. Bilz, and D. Bäuerle, Phys. Rev. Lett. **37**, 1155 (1976).
[14]B. N. N. Achar, G. R. Barsch, and L. E. Cross, Phys. Rev. B **24**, 1209 (1981).
[15]A. G. Beattie and G. A. Samara, J. Appl. Phys. **42**, 2376 (1971).
[16]M. A. Breazeale, J. Philips, A. Zarembovitch, M. Fischer, and Y. Gesland, J. Sound Vib. **88**, 133 (1983).
[17]E. R. Naimon and A. V. Granato, Phys. Rev. B **7**, 2091 (1973).
[18]L. E. A. Jones, Phys. Chem. Min. **4**, 23 (1979).
[19]Wenwu Cao, G. R. Barsch, W. Jiang, and M. A. Breazeale, Phys. Rev. B (to be published).
[20]K. S. Aleksandrov, L. M. Reshchikova, and B. V. Beznosikov, Phys. Status Solidi **18**, K17 (1966); Fiz. Tverd. Tela. (Leningrad) **8**, 3637 (1966) [Soviet Physics–Solid State **8**, 2904 (1967)].
[21]R. L. Melcher and R. H. Plovnick, in *Phonons,* edited by M. A. Nusimovici (Flammarion, Paris, 1971), p. 348.
[22]K. Fossheim, D. Martinsen, and A. Linz, in *Anharmonic Lattices, Structural Transitions, and Melting,* edited by T. Riste (Noordhoff, Leiden, 1974), p. 141.
[23]H. Hahn, in *Inelastic Scattering of Slow Neutrons from Solids and Liquids* (IAEA, Vienna, 1963), Vol. 1, p. 37.
[24]G. Leibfried and W. Ludwig, in *Solid State Physics,* edited by F. Seitz and D. Turnbull (Academic, New York, 1961), Vol. 12, p. 275.
[25]P. Carcia and G. R. Barsch, Phys. Rev. B **8**, 2505 (1973).
[26]E. H. Bogardus, Ph.D. thesis, The Pennsylvania State University, 1964.
[27]H. J. McSkimin, J. Acoust. Soc. Am. **33**, 12 (1961); **33**, 606 (1961); **37**, 864 (1965).
[28]R. N. Thurston and K. Brugger, Phys. Rev. **133**, A1604 (1964).
[29]H. Sakashita and N. Omaha, Phase Trans. **2**, 263 (1982).
[30]Z. P. Chang and G. R. Barsch, J. Geophys. Res. **78**, 2418 (1973).
[31]G. R. Barsch, Phys. Status Solidi **19**, 129 (1967).
[32]G. R. Barsch and Z. P. Chang, J. Appl. Phys. **39**, 3276 (1968).
[33]Z. P. Chang and G. R. Barsch, Phys. Rev. Lett. **19**, 1381 (1967).
[34]K. Fossheim and B. Berre, Phys. Rev. B **5**, 3292 (1972).
[35]K. Fossheim and R. M. Holt, Phys. Rev. Lett. **45**, 730 (1980).
[36]U. T. Höchli and A. D. Bruce, J. Phys. C **13**, 1963 (1980).
[37]E. Pytte, in *Structural Phase Transitions and Soft Modes,* edited by E. J. Samuelsen, E. Andersen, and J. Feder (Universitätsforlaget, Oslo, 1971).
[38]W. Rehwald, Phys. Kondens. Mater. **14**, 21 (1971).
[39]A. Aharoni and A. D. Bruce, Phys. Rev. Lett. **33**, 427 (1974).
[40]K. Gesi, J. D. Axe, G. Shirane and A. Linz, Phys. Rev. B **5**, 1933 (1972).
[41]T. Nattermann, J. Phys. C **9**, 3337 (1976).
[42]J. C. Slater, *Introduction to Chemical Physics* (McGraw-Hill, New York, 1939).
[43]K. Brugger and T. Fritz, Phys. Rev. **157**, 524 (1967).
[44]R. A. Cowley, Phys. Rev. **134**, A981 (1964).
[45]When the effective ionic charges and the other shell-model parameters are fitted both to elastic constants and phonon-dispersion data, significantly different values than these free-ion values can be obtained (Ref. 11). Since cohesive energies of ionic crystals are generally accounted for best with free-ion charges it seems more plausible, however, to use these values for elastic constant calculations, unless deformation-induced charge-transfer effects are included which go beyond the rigid shell model.
[46]M. P. Tosi, in *Solid State Physics,* edited by F. Seitz and D. Turnbull (Academic, New York, 1964), Vol. 16, p. 1, Table IX. Since our analysis is intended to be only approximate we neglect the van der Waals contributions included in the Huggins-Mayer treatment.
[47]J. Y. Gesland, M. Binois, and J. Nouet, C. R. Acad. Sci. (Paris) B **275**, 551 (1972).
[48]R. L. Melcher and D. I. Bolef, Phys. Rev. **178**, 864 (1969).
[49]R. Almairac, M. Rousseau, J. Y. Gesland, J. Nouet, and B. Hennion, J. Phys. (Paris) **38**, 1429 (1977).
[50]M. Rousseau, J. Y. Gesland, J. Julliard, J. Nouet, J. Zarembovitch, and A. Zarembovitch, Phys. Rev. B **12**, 1579 (1975).
[51]R. E. Watson, Phys. Rev. **111**, 1108 (1958).
[52]L. A. Feldkamp, J. Phys. Chem. Solids **33**, 711 (1972).
[53]R. Srinivasan, G. Laxmi, and V. Ramachandran, J. Phys. C **8**, 2889 (1975); **8**, 2897 (1975).
[54]M. Rousseau, J. Phys. Lett. **40**, L439 (1979).
[55]J. Y. Buzare and P. Simon, J. Phys. C **17**, 2681 (1984).
[56]E. R. Naimon, Phys. Rev. B **9**, 737 (1974).